nature chemical biology

ARTICLES

https://doi.org/10.1038/s41589-018-0060-1

Identification of a *S. aureus* virulence factor by activity-based protein profiling (ABPP)

Christian S. Lentz[1,6], Jessica R. Sheldon[2,6], Lisa A. Crawford[3], Rachel Cooper[4], Megan Garland[1], Manuel R. Amieva[4,5], Eranthie Weerapana[3], Eric P. Skaar[2] and Matthew Bogyo[1,5*]

Serine hydrolases play diverse roles in regulating host–pathogen interactions in a number of organisms, yet few have been characterized in the human pathogen *Staphylococcus aureus*. Here we describe a chemical proteomic screen that identified ten previously uncharacterized *S. aureus* serine hydrolases that mostly lack human homologs. We termed these enzymes fluorophosphonate-binding hydrolases (FphA–J). One hydrolase, FphB, can process short fatty acid esters, exhibits increased activity in response to host cell factors, is located predominantly on the bacterial cell surface in a subset of cells, and is concentrated in the division septum. Genetic disruption of *fphB* confirmed that the enzyme is dispensable for bacterial growth in culture but crucial for establishing infection in distinct sites in vivo. A selective small molecule inhibitor of FphB effectively reduced infectivity in vivo, suggesting that it may be a viable therapeutic target for the treatment or management of *Staphylococcus* infections.

The bacterium *S. aureus* is a highly significant human pathogen and a major cause of bacterial infections worldwide[1]. While this bacterium is found as part of the commensal skin and mucosal microbiome in about 30% of the human population, it is usually held in check by the physical barrier of the skin. However, upon breach of host defenses, *S. aureus* can disseminate systemically, leading to life-threatening conditions such as endocarditis, osteomyelitis, meningitis and sepsis[2]. *S. aureus* often forms highly robust biofilms in which the bacterium populates synthetic surfaces, for example, on prosthetic devices, surrounding itself in a biomolecular matrix that is largely impermeable to the immune system and many antibiotics, causing infections that are complicated and costly to monitor and treat[3]. Finally, an increased prevalence of community-acquired infections with antibiotic-resistant strains[2] is a further reason why *S. aureus* remains a major human health threat that requires new methods for rapid detection, treatment and therapy response monitoring.

Hydrolytic enzymes have vital roles for maintaining bacterial homeostasis and survival at the host–pathogen interface[4–10] and thus represent potential antivirulence and anti-infectivity targets[11,12]. Serine hydrolases are one of the largest and most diverse enzyme classes in eukaryotic and prokaryotic proteomes[13]. One of the largest subgroups of serine hydrolases, the α,β-hydrolases, are classified as enzymes that play important roles in processing of metabolites, peptides and lipids as a means of controlling cell signaling and metabolism. They also have been proven to be effective drug targets for a variety of diseases[14–16], yet the functionalities of α,β-hydrolases in *S. aureus* remain largely unknown.

Serine hydrolases proceed through an acyl enzyme intermediate during processing of a substrate, and thus a range of serine-reactive electrophiles can be used to covalently target these enzymes[17]. In fact, fluorophosphonate-based probes have been used to globally profile serine hydrolases in animal tissues[11,18], human cell lines[19], the pathogenic bacteria *Mycobacterium tuberculosis*[20,21] and *Vibrio cholerae*[22], and Archaea[23]. Here we describe a functional proteomic screen in live *S. aureus* under biofilm-promoting conditions using the serine-reactive activity-based probe (ABP) fluorophosphonate tetramethylrhodamine (FP-TMR)[12]. This screen identified a set of ten α,β-hydrolase-containing enzymes that are expressed in live *S. aureus* that have little or no homology to host-derived serine hydrolases. Through the identification and use of a covalent inhibitor, development of a highly selective fluorescent ABP and the use of genetic knockout strains, we were able to characterize one of these hydrolases as a virulence factor. This enzyme is localized at the bacterial surface, is heterogeneously distributed in the bacterial population, can process short-chain lipid esters, is regulated in response to host-cell derived factors and is important for infection of distinct tissue sites in vivo. Our results demonstrate the power of a focused functional proteomic screen in a relevant human pathogen such as *S. aureus* to identify a group of hydrolytic enzymes whose functions are likely to be important for various aspects of cellular physiology and host–pathogen interaction. Given their accessibility to modification by chemical probes and lack of human homologs, these enzymes may be promising targets for diagnosis, monitoring or treatment of *S. aureus* infections.

Results

Serine hydrolase activity profiling and inhibitor screen. Global profiles of serine hydrolase activity can be generated by treating intact cells with the fluorescent ABP FP-TMR followed by analysis of labeled protein by SDS–PAGE analysis (Fig. 1a). ABPs also allow screening for inhibitors of newly identified enzyme targets without the need to express the enzymes and identify substrates by competition labeling (Fig. 1b). Therefore, we set out to identify new serine hydrolase targets in *S. aureus* using the FP-TMR probe. Since the biofilm form of *S. aureus* is highly clinically relevant, we performed initial activity-based protein profiling (ABPP) with FP-TMR in *S. aureus* cells (strain ATCC3556) that were grown under biofilm-

[1]Department of Pathology, Stanford University School of Medicine, Stanford, CA, USA. [2]Department of Pathology, Microbiology and Immunology, Vanderbilt University Medical Center, Nashville, TN, USA. [3]Department of Chemistry, Boston College, Chestnut Hill, MA, USA. [4]Department of Pediatrics, Stanford University School of Medicine, Stanford, CA, USA. [5]Department of Microbiology and Immunology, Stanford University School of Medicine, Stanford, CA, USA. [6]These authors contributed equally: Christian S. Lentz, Jessica R. Sheldon. *e-mail: mbogyo@stanford.edu

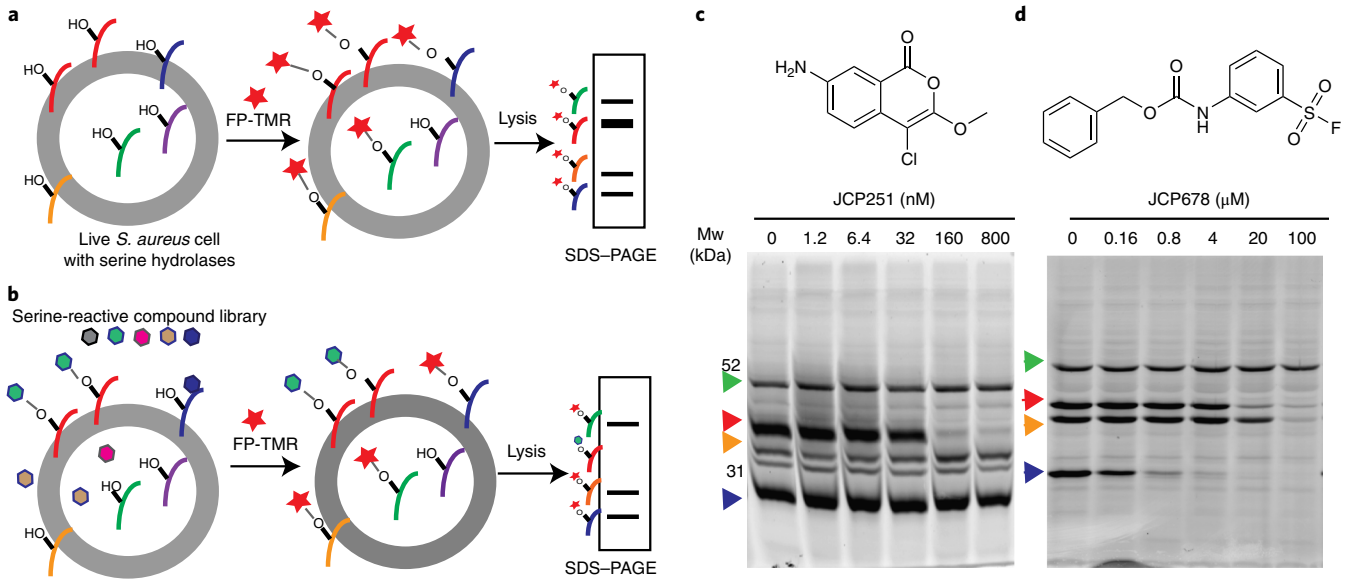

Fig. 1 | Identification of serine hydrolases and inhibitors in live *S. aureus* by competitive ABPP. a, Schematic of serine hydrolase labeling in live *S. aureus* with FP-TMR (red star) followed by SDS–PAGE analysis to detect labeled targets. **b**, Schematic overview of competitive ABPP platform to identify selective inhibitors of individual hydrolases from a library of small molecules (hexagons). **c**, Chemical structure of JCP251 and SDS–PAGE analysis of *S. aureus* lysates after live cells were incubated with JCP251 or vehicle control (1% DMSO) before FP-TMR labeling. Arrowheads indicate consistently observed serine hydrolase activities. Mw, molecular weight. **d**, Chemical structure of JCP678 and its FP-TMR competition-labeling profile in *S. aureus*. Experiments shown in **c**,**d** were repeated twice with similar results.

promoting conditions, removed from the matrix and suspended in broth. This identified multiple prominently labeled enzymes that were resolved by SDS–PAGE analysis of the total cellular lysates (Fig. 1c). Without knowing the identity of these targets, we screened a library of ~500 compounds that were designed to covalently target serine proteases and hydrolases[24,25] using the competition labeling method (Supplementary Fig. 1a and Supplementary Table 1). Deconvolution of the original screening mixtures and secondary screening of individual compounds identified potent and selective inhibitors of two of the most efficiently labeled hydrolases (Supplementary Fig. 1b and Supplementary Table 1). Specifically, compound **1**, the chloroisocoumarin JCP251, was selective for a ~36 kDa hydrolase target at nanomolar concentrations (Fig. 1c) and compound **2**, the sulfonyl fluoride JCP678, showed selectivity for a ~28 kDa hydrolase at low micromolar concentrations (Fig. 1d).

To identify the targets of these inhibitors along with the other probe-labeled *S. aureus* serine hydrolases, we pretreated live bacteria with JCP251, JCP678 or vehicle control and then labeled them with the biotin-tagged probe FP-biotin. Cells were lysed and enriched for biotinylated proteins using a streptavidin resin, and samples were analyzed by LC/LC-MS/MS (Fig. 2a). Using this strategy, we identified peptides from 12 proteins predicted to contain an α,β-hydrolase domain (Supplementary Table 2 and Supplementary Dataset 1; data available via ProteomeXchange with identifier PXD009210). All of these proteins, with the exceptions of *S. aureus* lipases SAL1 and SAL2[26–28], are poorly annotated, with no assigned cellular functions. We then examined the predicted domain structures, cellular location, size and closest human homologs of each of the 12 hydrolases (Fig. 2a). Given that none of the enzymes (except SAL1 and SAL2) have been given names or have identifiable human homologs, we named these 10 enzymes "fluorophosphonate-binding serine hydrolases" (Fphs) following the nomenclature used for penicillin-binding proteins. We assigned sequential letters (A–J) to each enzyme based on the predicted size of the proteins, with the largest protein being assigned the letter A. Two of these uncharacterized hydrolases, FphE and FphG, were previously reported (but not named or further studied) in a chemoproteomic study using β-lactam probes that primarily target penicillin-binding proteins[6,29]. None of the other Fph targets were labeled by the β-lactam probes[6]. By identifying specific hydrolases whose recovery was blocked by pretreatment with the selective inhibitors, we identified the 36-kDa hydrolase as FphB and the primary target of JCP251, and the 28 kDa protein as FphF and the target of JCP678 (Fig. 2b,c, Supplementary Fig. 2, Supplementary Table 2 and Supplementary Dataset 1).

To further confirm the identity of all of the major FP-TMR-labeled hydrolases, we obtained strains from the Nebraska Transposon Mutant Library[30] with insertions in individual *fph* genes. We transduced these mutants into the well-characterized *S. aureus* Newman laboratory strain background and performed FP-TMR labeling experiments to correlate individual hydrolases with probe-labeled proteins by SDS–PAGE analysis (Fig. 2d). For transposon mutants strains deficient in either SAL1, SAL2, FphA, FphB, FphE, FphF or FphH, we observed loss of a labeled species of the corresponding molecular weight from the FP-TMR labeled proteome. For the *fphD* mutant, we observed loss of labeling of a hydrolase of < 30 kDa, which is smaller than the expected size of 33 kDa, but is consistent with a previous observation[6]. Among the available transposon mutant strains, we were not able to identify FphC and FphG as probe-labeled bands in the SDS–PAGE gel. This might be due to the low abundance of these enzymes in combination with lower sensitivity and limited resolution of the SDS–PAGE compared to the MS-based assay, as well as different activity and permeability of the biotinylated and fluorescent probes. Notably, the *fphH* transposon mutant displayed elevated labeling of several other serine hydrolase activities (for example, FphE and FphD), suggesting a possible level of functional redundancy and/or compensation among these enzymes (Fig. 2d). Ultimately, we were able to identify eight Fphs, SAL1 and/or SAL2, as well as three additional labeled proteins in the SDS–PAGE experiment whose identities have yet to be confirmed (Fig. 2e).

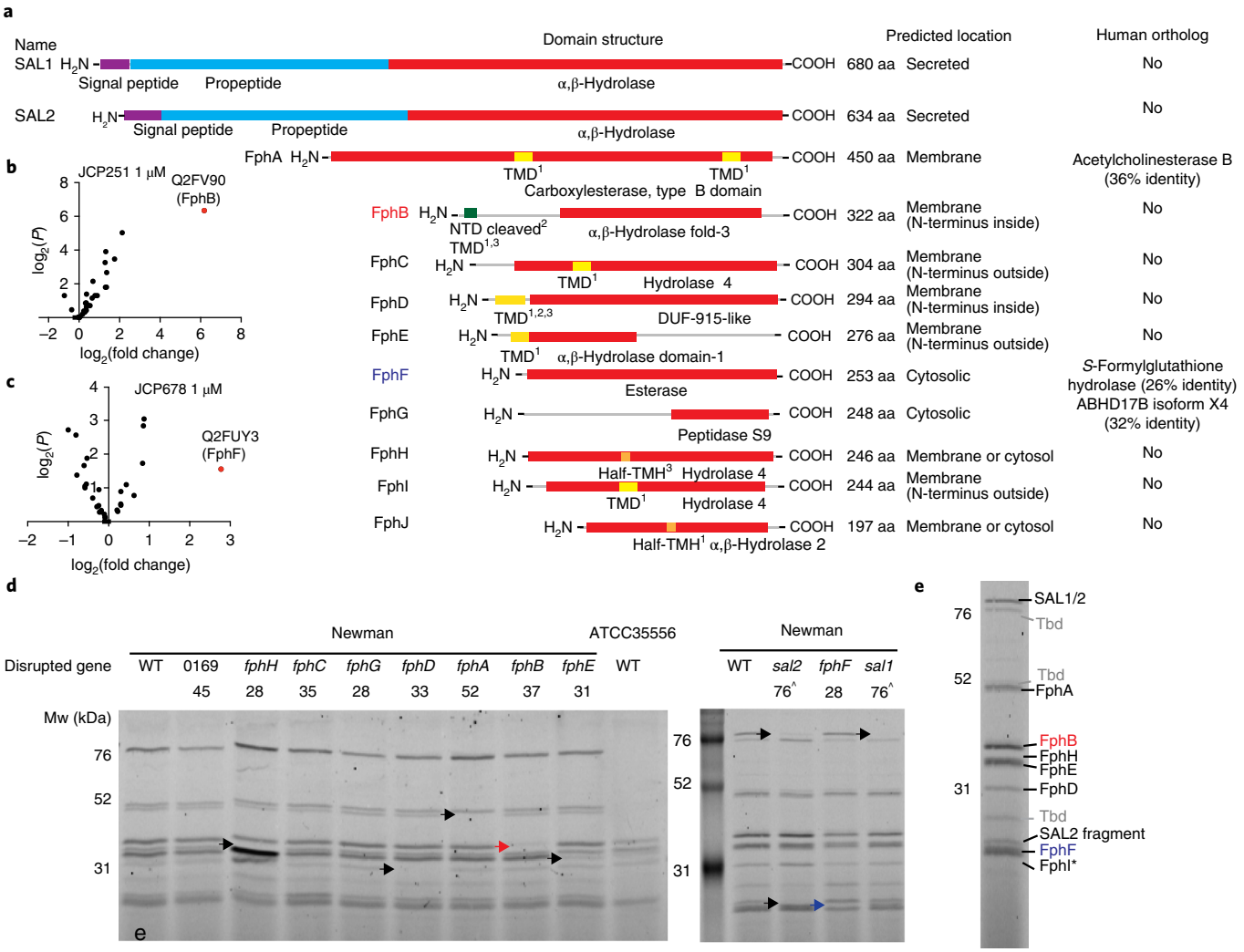

Fig. 2 | LC/LC-MS/MS-based identification of serine hydrolases in *S. aureus*. a, Domain structure prediction and bioinformatics analyses of identified hydrolases. Red: α,β-hydrolase domain (family specification according to Pfam). Purple: signal peptides. Cyan: propeptides. Yellow: transmembrane domain (TMD). Orange: possible half-transmembrane-helix (half-TMH). Green: ambiguous N-terminal domain (NTD). The programs predicting the presence of a TMD or TMH are indicated as follows: [1]TmPred, [2]Phobius, [3]MemBrain. For identification of human orthologs by BLASTp, the nonredundant protein sequences database for *Homo sapiens* was queried using the indicated full-length protein sequences. **b**,**c**, Volcano plot of FP-biotin targets in *S. aureus* ATCC35556 showing change in recovery upon JCP251 (**b**) and JCP678 (**c**) pretreatment relative to a control. The top hit (most significant change in recovery) is labeled. Two-tailed *t*-test on $n = 3$ biologically independent samples for each of the two groups being compared. **d**, FP-TMR labeling profiles of *S. aureus* Newman transposon mutant strains with insertions in serine hydrolase genes. Arrowheads indicate labeled proteins disappearing in individual mutant strains (red arrowhead, FphB; blue arrowhead, FphH). The experiment was performed twice with similar results. **e**, The primary labeled targets of FP-TMR in *S. aureus* Newman. Identities of species confirmed by mutational analysis are indicated. Asterisk indicates that FphI identity is predicted on the basis of molecular weight (Mw). "Tbd" indicates that the identity remains unconfirmed.

Biochemical analysis of *S. aureus* FphB. Although we identified ten serine hydrolases in our proteomic screen that each likely serve important functions to the bacteria, we focused our initial efforts on FphB because of its overall high activity in cells, lack of prior characterization and the overall potency and selectivity of the JCP251 lead inhibitor. FphB is predicted to be a 322 amino acid protein of 36.8 kDa (Fig. 2a). Bioinformatic analyses suggest that FphB does not have a classical signal peptide, is not secreted, but may possess a short N-terminal transmembrane domain or cleavage site (Supplementary Table 3). Data mining of previously published transcriptomic datasets revealed that *fphB* gene transcription is moderately upregulated (1.8–2.9-fold) upon exposure to various cell-wall-acting antibiotics and antimicrobial peptides (locus tags SA2323[31–33] and SA2549[34], respectively). Similar upregulations in *fphB* transcription are found in response to neutrophil-associated azurophilic granules, hydrogen peroxide, hypochlorus acid (locus tag MW2456)[35], acid shock (locus tag SA2549)[36] and antibacterial skin fatty acids (temporary upregulation, locus tag SA2323)[37], suggesting a potential role for FphB under stress conditions at the host–pathogen interface. We recombinantly expressed FphB and purified it as the full length, His_6- and T7-tagged fusion protein rFphB from *Escherichia coli* (Supplementary Fig. 3). To determine whether the protein was enzymatically active, we tested a panel of commercially available fluorogenic substrates (Fig. 3a). We found that the rFphB protein cleaved fluorogenic esterase substrates, but did not process phosphate, phosphonate or glycosidic substrates or the protease substrate FITC-casein (Fig. 3b). Among the ester substrates tested, it preferred $C_4 > C_7 > C_8$ fatty acid esters but was unable to cleave C_2, C_{10} or longer fatty acid esters. Using 4-methylumbelliferyl butyrate as a substrate, we measured the inhibitory activity of JCP251

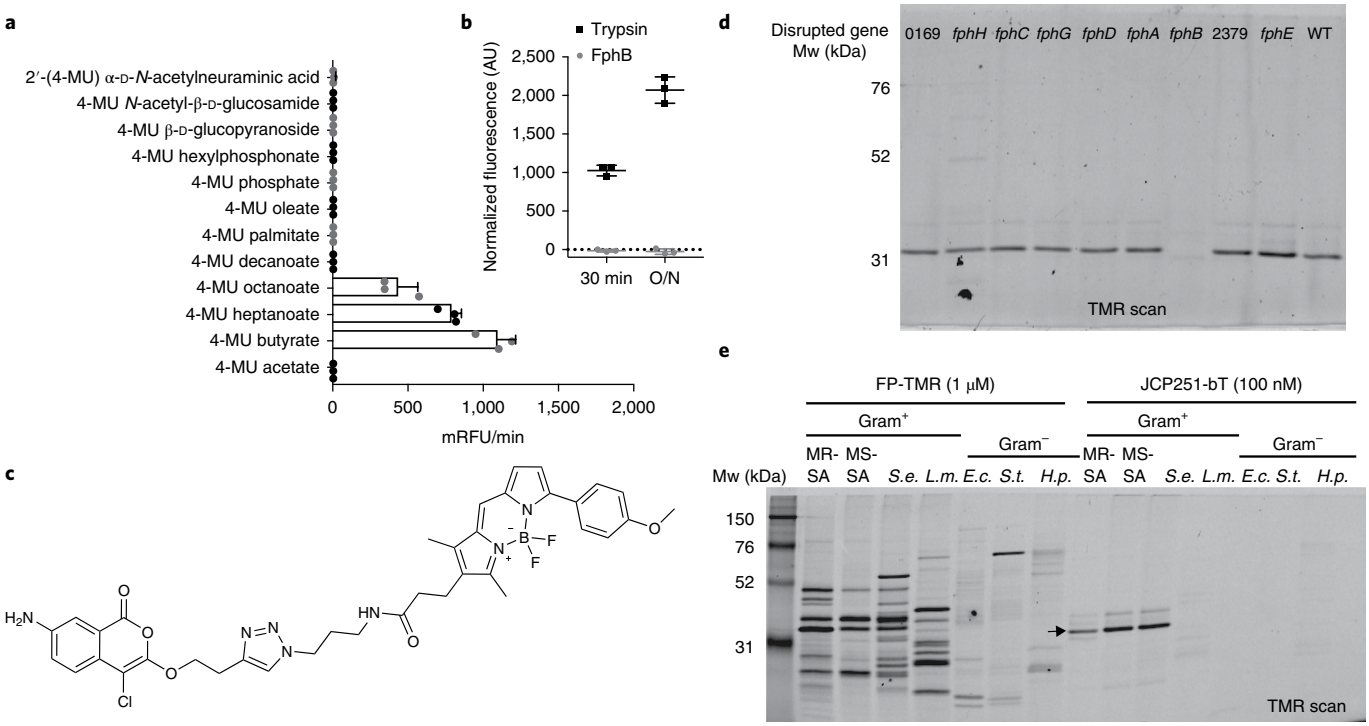

Fig. 3 | Biochemical characterization of FphB and development of an FphB-selective fluorescent ABP. a, Processing of 4-methylumbelliferyl (4-MU)-based fluorogenic substrates by rFphB. Turnover rates for each substrate are depicted as milli-RFU (relative fluorescence units)/min. Graph shows individual values overlaid with the means ± s.d. of 3 biologically independent samples. **b**, Proteolytic activity of rFphB or trypsin against FITC-casein depicted as normalized fluorescence in arbitrary units (AU). Graph shows an overlay of individual values and means ± s.d., $n = 3$ biologically independent samples. Raw data were normalized by subtracting background fluorescence under buffer control conditions. O/N, overnight. **c**, Chemical structure of the fluorescent ABP JCP251-bT. **d**, SDS–PAGE analysis (TMR fluorescence scan) of *S. aureus* Newman transposon mutant strains with insertions in indicated genes labeled with 100 nM JCP251-bT during exponential growth. Full gel image in Supplementary Fig. 4b. **e**, SDS–PAGE analysis of indicated Gram-positive and Gram-negative bacterial pathogens labeled with FP-TMR or JCP251-bT. MR-SA: *S. aureus* USA300, MS-SA: *S. aureus* ATCC35556, *S.e.*: *S. epidermidis*, *L.m.*: *Listeria monocytogenes*, *E.c.*: *Escherichia coli*, *S.t.*: *Salmonella typhimurium*, *H.p.*: *Helicobacter pylori*. Arrow indicates FphB. All experiments were repeated twice with similar results.

against rFphB and found that it had a fast inactivation rate $k_{obs}/[I]$ of $8.5 \pm 1.6 \times 10^6\ M^{-1}\ s^{-1}$, consistent with its ability to block labeling of FphB even at nanomolar concentrations in the competition labeling studies.

A fluorescent activity-based probe for *S. aureus* FphB. JCP251 is an ideal starting point for the design of an ABP for imaging of FphB activity in live bacteria. Our set of screening hits indicated that substitution of the C_3 methoxy group by a propyloxy or isopropyloxy moiety (compound **3** (JCP174) and compound **4** (JCP222), respectively, in Supplementary Fig. 1) largely retained the activity profile of JCP251. We therefore tested an analog of JCP251 containing the bodipy-TMR fluorophore attached through a linker at the C3 methoxy substitution (compound **5** or JCP251-bT; Fig. 3c)[38]. This fluorescent probe had similar potency compared to the parent JCP251 inhibitor with only a ~3-fold lower inactivation rate ($k_{obs}/[I] = 2.6 \pm 1.8 \times 10^6\ M^{-1}\ s^{-1}$). When JCP251-bT was applied to *S. aureus* cultures, it labeled a single protein that was observed throughout exponential and stationary phase growth in liquid culture (Supplementary Fig. 4a). This specific labeling was lost in the *fphB* transposon mutant strain, confirming the high selectivity of the probe for FphB in live cells (Fig. 3d and Supplementary Fig. 4b). The probe labeled a small number of potential off targets when applied to the soluble fraction of bacterial lysates instead of live cells (Supplementary Fig. 4c). This result could be due to limited membrane permeability of the probe or the release and activation of hydrolase targets under lysis conditions.

To further assess the selectivity of JCP251-bT for *S. aureus* FphB over related hydrolases in other bacteria, we used the probe to label various Gram-positive and Gram-negative bacteria (Fig. 3e). All of these bacteria expressed multiple serine hydrolase activities that were detected by the broad-spectrum FP-TMR probe. We performed homology searches for FphB and found orthologs with 53–57% identity in other *Staphylococcus* species, while putative orthologs in other prokaryotic and eukaryotic organisms showed only 25–39% identity (Supplementary Fig. 5a). Accordingly, JCP251-bT labeled methicillin-sensitive and methicillin-resistant *S. aureus* (MRSA) strains, as well as *S. epidermidis*, but did not show any labeling of targets in several other bacterial pathogens. To assess whether JCP251-bT is sufficiently selective for FphB to be used for imaging during an infection, we performed labeling studies of live bacteria cocultured with peripheral mononuclear cells and mouse RAW264.7 macrophage cells. The probe weakly labeled proteins in both host cell types alone, but upon co-incubation of these cells with *S. aureus*, it predominantly labeled FphB (Supplementary Fig. 5c) and allowed visualization of probe-labeled bacteria over weak background fluorescence caused by nonspecific probe uptake and/or labeling of host cell proteins (Supplementary Fig. 5d).

FphB activity is dynamically regulated. Given that expression levels of the *fphB* gene may be altered by skin-derived signals[37], we wanted to determine whether activity levels (as measured by the JCP251-bT probe) responded to host cell derived factors. We observed that FphB labeling by JCP251-bT was significantly

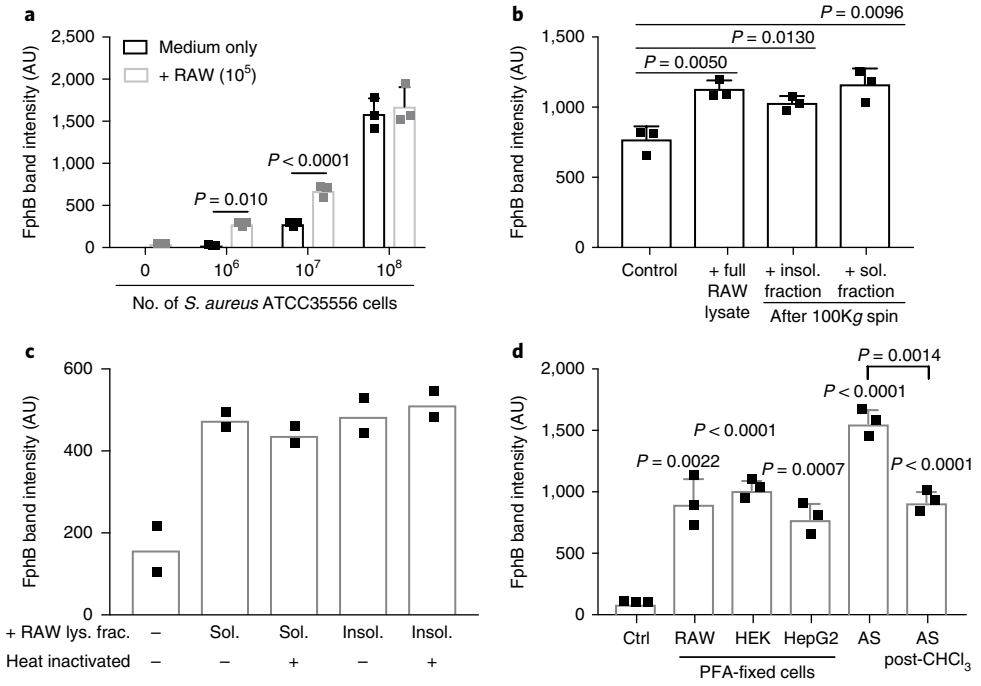

Fig. 4 | Stimulatory activity of eukaryotic cell components on FphB activity. All graphs show FphB activities in *S. aureus* cells in response to the indicated stimuli. After stimulation, active FphB in live cells was labeled with JCP251-bT (100 nM) before lysates were analyzed by SDS–PAGE and FphB band intensities were quantified using Image Studio Lite. **a**, FphB band intensity in *S. aureus* ATCC35556 grown individually or in coculture with RAW cells at the indicated cell numbers. Graph shows means ± s.d. of 3 biologically independent samples. Unpaired, two-tailed Student's *t*-test. See Supplementary Fig. 6a for full gel. **b**, FphB band intensity after *S. aureus* ATCC35556 (1×10^7 CFU) were grown in the presence of full RAW cell lysate or the insoluble (insol.) or soluble (sol.) fractions (each equivalent to 1×10^5 cells) after ultracentrifugation before JCP251-bT labeling (see Supplementary Fig. 6b for full gel). Graph shows means ± s.d. of 3 biologically independent samples. Unpaired, two-tailed Student's *t*-test. **c**, FphB band intensity after *S. aureus* ATCC35556 were treated with heat-inactivated or untreated soluble or insoluble lysate fractions (lys. frac.) after ultracentrifugation before JCP251-bT labeling. Graph shows means of 2 biologically independent samples. See Supplementary Fig. 6d for full gel. **d**, FphB band intensity after *S. aureus* Newman WT were incubated with PFA-fixed RAW, HEK or HepG2 cells, 10% Fetal Animalplex Serum (AS) or 10% AS after chloroform extraction before labeling with JCP251-bT. See Supplementary Fig. 6g for full gel with *fphB*::ϕNΣ controls. Graph shows means ± s.d. of 3 biologically independent samples. Unpaired, two-tailed Student's *t*-test.

increased in the presence of RAW cells and that the extent of this effect was dependent on the ratio of bacterial cells to host cells (Fig. 4a and Supplementary Fig. 6a). This ratio dependency might be explained by a contact-dependent mechanism whereby at high bacterial density the necessary contact points on the macrophage surface are saturated, resulting in a lower net stimulation per bacterium. This stimulatory effect was retained in both soluble and insoluble fractions from RAW cell lysates, as well as in PFA-fixed cells (Fig. 4b,c and Supplementary Fig. 6b–e). Our data suggest that the increase in FphB activity is not dependent on active metabolic processes in the host cell, but is rather mediated through contact with a heat-stable component on the RAW cell surface. Notably, we did not observe any secretion of FphB into the culture medium (Supplementary Fig. 6f). Furthermore, the effect was not specific for macrophages. Bacteria reacted similarly to exposure to PFA-fixed human hepatocellular carcinoma (HepG2) and PFA-fixed human embryonic kidney (HEK) cells, as well as to Fetalplex Animal Serum Complex (Gemini Bio-Products). Notably, the stimulatory components in the serum could partially be depleted by chloroform extraction, suggesting they may be lipids or fatty acids (Fig. 4d and Supplementary Fig. 6g). Together, these data suggest that *S. aureus* (both strains ATCC35556 and Newman) regulates FphB activity in response to host-cell-derived signals.

FphB labeling in the cell envelope is asymmetric and heterogenous. As the location of a protein provides clues to its physiological function, we sought to experimentally determine the location of enzymatically active FphB in the bacterium by labeling with JCP251-bT. To confirm probe specificity, we used flow cytometry to quantify labeling on a population scale in both wild-type (WT) and *fphB* transposon mutant bacteria (Fig. 5a,b and Supplementary Fig. 7). JCP251-bT labeling was detected in Newman WT and FphE-mutant populations, while for both the FphB-deficient bacteria and WT bacteria pretreated with JCP251 we only could detect background autofluorescence. Notably, the probe labeled only ~7–10% of Newman WT cells, and a higher percentage of cells were probe-positive in the FphE-deficient strain. This suggests that FphB is heterogeneously expressed among individual cells in the bacterial population. Confocal fluorescence microscopy experiments in Newman cells again confirmed that JCP251-bT labeling was specific to FphB (Fig. 5c). To better localize FphB activity, we probe-labeled a Newman strain expressing a GFP reporter. We observed that FphB activity levels varied dramatically among individual WT cells (Fig. 5d), and, as expected, pretreatment with JCP251 reduced fluorescent signals to background levels (Supplementary Fig. 8). Notably, JCP251-bT labeling did not colocalize with the cytosolic GFP signal but rather showed concentrated signals in specific regions of the cell envelope (Fig. 5d–g). Furthermore, a subset of dividing cells showed enriched probe labeling in the septal cross-wall, the primary location of cell wall biogenesis in *S. aureus* (Fig. 5g,h), suggesting that FphB might modify substrates located in the bacterial cell wall.

FphB is important for infection of distinct tissue sites in vivo. Given that FphB activity is concentrated in the cross-wall of dividing cells, we reasoned that it might be important for cell division.

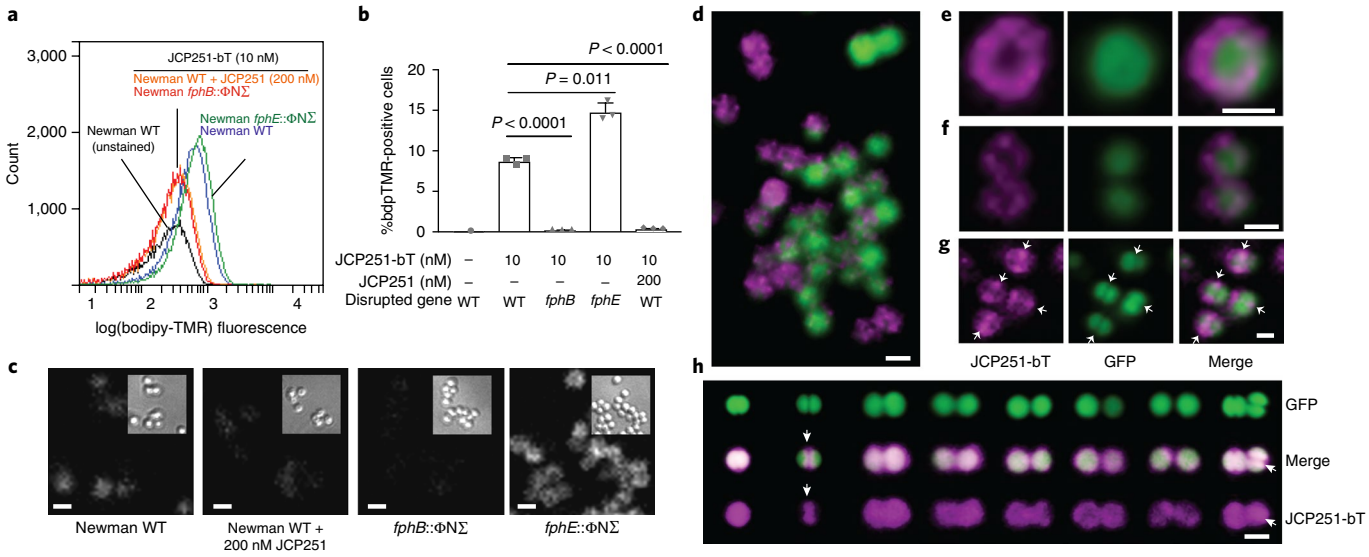

Fig. 5 | Imaging of FphB-activity using the fluorescent ABP JCP251-bT. a, Flow cytometry plot of JCP251-bT probe fluorescence in *S. aureus* Newman WT, *fphB*::ϕNΣ and *fphE*::ϕNΣ strains treated with FphB-inhibitor JCP251 or vehicle before labeling with JCP251-bT during exponential growth. **b**, Percentage of cells in the bodipy-TMR (bdpTMR)-positive gate (see gating strategy in Supplementary Fig. 8). Graph shows means ± s.d. of 3 biologically independent samples. Unpaired, two-tailed Student's *t*-test. **c**, Confocal micrographs of indicated *S. aureus* strains labeled with 10 nM JCP251-bT. bT fluorescence is depicted in white; insets show differential interference contrast images. **d**, 3D reconstruction of a series of confocal images of *S. aureus* Newman-GFP labeled with 10 nM JCP251-bT. GFP fluorescence: green, bT fluorescence: purple. **e**,**f**, Confocal micrographs of *S. aureus* Newman-GFP cell labeled with 10 nM JCP251-bT during exponential phase. **g**, Confocal micrograph of dividing *S. aureus* Newman-GFP labeled with 10 nM JCP251-bT during stationary phase. Arrows indicate division septum plane. **h**, 3D reconstructions of confocal image series of *S. aureus* Newman-GFP cells labeled with 10 nM JCP251-bT during stationary phase. Examples of cells in different stages of cell division are shown. Enriched JCP251-bT labeling of the division septum is marked by white arrows. All scale bars: 1 μm. All experiments were repeated twice with similar results.

We therefore monitored the fitness of the *fphB* transposon mutant during in vitro growth. Surprisingly, the FphB-deficient strain had no growth defect in liquid culture (Fig. 6a) and showed a similar doubling time (55.4 ± 3.5 min) to the WT (55.9 min ± 1.5 min). Furthermore, treatment of WT bacteria with JCP251 to chemically block FphB activity did not alter bacterial growth either (Fig. 6a). Given these results, and the fact that FphB activity levels are dynamic and change in response to host cell derived factors, we reasoned that it may be functionally important during infection of a host organism. Using a mouse model of systemic infection, we observed that mice infected with the *fphB* transposon mutant strain had ~10- to 100-fold lower bacterial loads than the WT strain in liver and heart tissues, but equal colony-forming unit (CFU) numbers in the kidneys (Fig. 6b). In contrast, infection with the *fphE* transposon mutant resulted in only a small, though statistically significant, reduction of bacterial loads in the liver, and no reduction in the hearts or kidneys of infected mice (Supplementary Fig. 9). The overall weight loss in the course of infection with either mutant strain was comparable to that of WT-infected mice (Supplementary Fig. 9). These findings suggest the existence of distinct molecular mechanisms for the colonization of these organs by *S. aureus* and establish FphB as important for the ability of *S. aureus* to infect heart and liver tissues.

Finally, we wanted to determine whether chemical inhibition of FphB before infection would negatively affect the pathogen's ability to establish tissue infection in vivo. We reasoned that pretreating cells with JCP251 would 'chemically knock down' FphB activity for early events during infection, but this effect would eventually be overcome by de novo expression of the protein in vivo. Pretreatment of *S. aureus* Newman with JCP251 before infection indeed reduced the bacterial burden in the liver to levels comparable to those observed upon infection with the *fphB* transposon mutant strain (Fig. 6c). In contrast, chemical knockdown of FphB before infection was insufficient to reduce CFU levels in the heart or kidneys (Fig. 6d,e). These data suggest a role for FphB activity during the early colonization or attachment phase of an intravenous infection.

Discussion

Although it is clear that serine hydrolases are important to various aspects of both bacterial and host cell biology, surprisingly little is known about this family of enzymes in *S. aureus*. This report describes the use of the serine-reactive electrophilic probe FP-TMR to identify putative serine hydrolase targets in *S. aureus*. Our profiling data confirm that *S. aureus* expresses several active serine hydrolases during normal and biofilm-like growth (in liquid culture and on agar), most of which are poorly characterized, lack annotation and have few, if any, mammalian homologs. The fact that this class of enzymes has so far largely escaped identification in in vitro phenotypic screens might be due to functional redundancy or functions at the host–pathogen interface that are difficult to capture with in vitro model systems.

Functional studies of one of these newly identified hydrolases, FphB, suggest that it responds to nonproteinaceous host-derived factors, is localized to the cell surface, as well as the division septum, and is important for the early stages of infection in vivo. The finding that disruption of FphB expression results in defects in infection of the heart and liver but not the kidneys suggests FphB may help bacteria to functionally adapt during colonization. The observed differences in infectivity for specific target organs could be linked to a molecular surface architecture that may require different strategies for attachment. Glycosaminoglycans are common receptors for bacterial attachment or other aspects of bacterial pathogenesis[39]. Murine kidney cells have been shown to have higher levels of glycosaminoglycans such as heparan sulfate than liver and heart tissues[40] and might thus facilitate FphB-independent tissue attachment. If FphB is in fact a key regulator of initial contact of

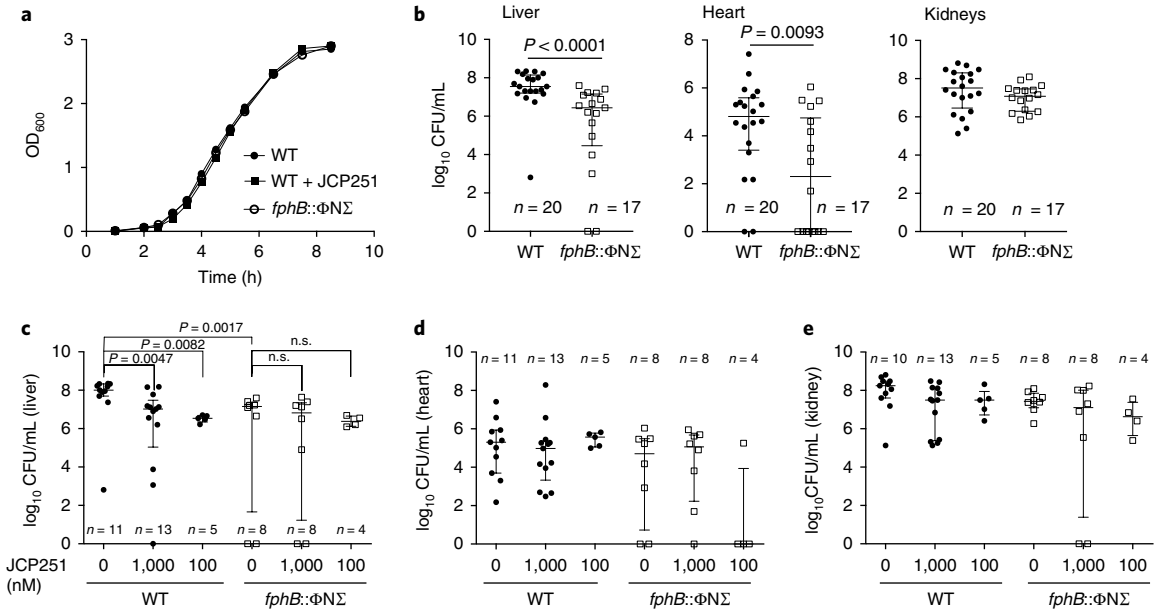

Fig. 6 | Effects of loss of FphB activity on infectivity in vivo. a, Growth curves of *S. aureus* Newman and its isogenic transposon mutant strain *fphB*::ϕNΣ and Newman WT in tryptic soy broth with or without 1 μM JCP251, as indicated. Graph shows means of 3 (WT) or 2 biologically independent cultures (WT + JCP251, *fphB*::ϕNΣ). **b**, Total CFU recovered from indicated organs of BALB/c mice 96 h after intravenous infection with *S. aureus* Newman WT or *fphB*::ϕNΣ. Graphs show pooled data (median ± interquartile range, WT: $n = 20$, *fphB*::ϕNΣ: $n = 20$) from 4 independent experiments. Unpaired, two-tailed Mann–Whitney test. **c**–**e**, Plots of total CFU recovered from indicated organs of BALB/c mice 96 h after systemic infection with *S. aureus* Newman WT and *fphB*::ϕNΣ that were pretreated with JCP251 or vehicle for 60 min. Graph shows pooled data (median ± interquartile range; sample sizes indicated in the graph) from 2 independent experiments. Kruskal–Wallis test of analysis of variance among each of these datasets revealed that only in the liver median CFU values varied significantly (liver: $P = 0.0058$, heart: $P = 0.1530$, kidneys $P = 0.0956$). Pairwise significance testing within the liver dataset (**c**) was done by unpaired, two-tailed Mann–Whitney test; n.s., not significant (between 0 and 1,000 nM, $P = 0.7423$; between 0 and 100 nM, $P = 0.2646$).

bacteria with host cells, it could represent an ideal target for small molecules that could prevent the spread of a primary infection to other sites that cause increased morbidity and mortality (i.e., heart valves and artificial implants).

Although active during all culture stages and conditions tested, we found increased levels of FphB activity after contact with structural components of eukaryotic cell membranes and lipophilic serum components. Such contact is likely to occur upon initial attachment to host cells during early stages of an infection, where FphB activity could promote the establishment of infection. Thus, after sensing a molecular environment corresponding to a certain niche, elevated FphB activity might represent one element of a dynamic functional response of the bacteria to colonize or survive in this new environment. As we observed FphB activity in only a subset of cells, our results suggest that *S. aureus* populations display a degree of functional diversity that might facilitate their survival in a variety of biological niches.

How FphB mediates such effects and what its physiological substrates are remain speculative. Our substrate profiling experiments with recombinant FphB suggest that the enzyme acts as a carboxylic acid esterase able to process C_4–C_8 chain fatty acid esters. Yet the true physiologic substrate(s) may not have been accounted for in the limited set of synthetic fluorogenic substrates tested. As FphB activity is increased in the presence of host-derived components, one possible scenario is that the enzyme processes exogenous biomolecules, allowing bacteria to scavenge host-derived substrates for their own metabolism. The ability to metabolize certain substrates may be key for survival in certain biological niches during infection or colonization (for example, heart and liver), but may not affect growth in rich liquid culture media or other tissue sites (for example, kidneys), consistent with our observations of the FphB mutant.

The potential endogenous substrate space includes the bacterial membrane and cell wall. As we did not observe cleavage of long chain fatty acid esters, we do not expect FphB to act on canonical membrane lipids. A first indication that FphB might directly act on substrates localized in the cell wall is the observed enrichment of JCP251-bT labeling in the cross-wall of dividing cells. The fact that several studies found *fphB* gene expression moderately upregulated in response to cell wall stress conditions induced by the antibiotics oxacillin[31] and daptomycin[34], cationic antimicrobial peptides[32] or the lantibiotic mersacidin[33] further links FphB activity to this cellular location. Enzymes known to act in the cross-wall of dividing cells are important for shaping the cell wall as a structural scaffold protecting the inside of the bacterial cell (for example, murein hydrolases)[7] or as an outward-facing matrix for interaction with the environment (for example, sortase A)[41]. Murein hydrolases are crucial for cell wall integrity and cell division, and mutations in their corresponding genes invoke severe growth phenotypes in vitro[7]. We did not observe a similar phenotype for the *fphB* mutant. In contrast, sortase A anchors secreted proteins with an LPXTG consensus sequence (for example, adhesins, protein A and further virulence factors) to the free amino terminus of pentaglycine in nascent peptidoglycan, and deficiency in sortase A attenuates pathogenicity in vivo[42]. Thus, sortase A is a prime example of a cell-surface-modifying enzyme whose functional relevance becomes evident in vivo, but not during growth in liquid culture. Similarly, FphB activity might govern environmental interactions by acting on cell-wall-anchored proteins or structural components of the cell wall. Structural modifications of cell wall polymers that have been reported to affect virulence, pathogenesis or colonization include O-acetylation at C_6 of *N*-acetylmuramic acid in peptidoglycan[43,44] and glycosylation[45] and D-alanylation[46] of wall teichoic acid. While biosynthetic routes for the main cell envelope polymers are mostly

well understood, evidence of enzymes involved in their dynamic modification or degradation is only emerging. Regulation of O-acetylation levels by the O-acetylpeptidoglycan esterase Ape, a serine hydrolase, has been described in different Gram-negative and Gram-positive bacteria, but not *S. aureus*[47,48], suggesting this function may be inherent to a previously uncharacterized hydrolase in this organism. A recent study on the *S. aureus* methicillin-resistance factor FmtA demonstrated that this enzyme acts as a teichoic acid-specific D-alanine esterase[49].

Notably, so-called functional membrane microdomains (FMMs) are also associated with septal invaginations of dividing cells. These dynamic membrane domains are organized through the scaffold protein flotillin, they are largely composed of saccharolipids derived from the carotenoid staphyloxanthin, and their integrity is required for the activity of the cell-wall-acting PBP2a, a mediator of penicillin resistance in MRSA[50]. Although FphB was not found among FMM-associated proteins in MRSA[50], it is conceivable that this enzyme acts on membrane-associated substrates in a regulatory fashion that translates into altered cell wall architecture with downstream effects on virulence. Given the multitude of described effects that individual cell envelope components have on bacterial virulence, regulated, dynamic chemical modifications of their structure through hydrolytic enzymes such as FphB appears to be a plausible strategy for bacteria to functionally adapt to their environment during infection or colonization.

The identification of FphB and the further set of nine uncharacterized Fph serine hydrolases by ABPP provides a starting point for future elucidation of their corresponding biological functions. Our study demonstrates that these enzymes are ideal targets for the development of selective inhibitors and activity-based probes that will facilitate the characterization of these hydrolase activities in their physiological environments. Given these initial functional studies of FphB, inhibition of this target may represent a new targeted strategy for preventing *S. aureus* colonization in major organs—for example, for prophylactic treatment of MRSA carriers before surgery. Furthermore, the ability to selectively label FphB with a small molecule fluorescent probe renders this enzyme a potential target for the development of targeted probes for localization and risk stratification of *Staphylococcus* spp. infections. These types of therapy and imaging agents could have a broad impact on diagnosis, treatment and therapy response monitoring for diverse types of *S. aureus* infection.

Methods

Methods, including statements of data availability and any associated accession codes and references, are available at https://doi.org/10.1038/s41589-018-0060-1.

Received: 18 October 2017; Accepted: 27 March 2018;
Published online: 16 May 2018

References

1. Reddy, P. N., Srirama, K. & Dirisala, V. R. An update on clinical burden, diagnostic tools, and therapeutic options of *Staphylococcus aureus*. *Infect. Dis. (Auckl.)* **10**, 1179916117703999 (2017).
2. Tong, S. Y., Davis, J. S., Eichenberger, E., Holland, T. L. & Fowler, V. G. Jr. Staphylococcus aureus infections: epidemiology, pathophysiology, clinical manifestations, and management. *Clin. Microbiol. Rev.* **28**, 603–661 (2015).
3. Laupland, K. B. et al. The changing epidemiology of *Staphylococcus aureus* bloodstream infection: a multinational population-based surveillance study. *Clin. Microbiol. Infect.* **19**, 465–471 (2013).
4. Duthie, E. S. & Lorenz, L. L. Staphylococcal coagulase; mode of action and antigenicity. *J. Gen. Microbiol.* **6**, 95–107 (1952).
5. Frees, D., Gerth, U. & Ingmer, H. Clp chaperones and proteases are central in stress survival, virulence and antibiotic resistance of *Staphylococcus aureus*. *Int. J. Med. Microbiol.* **304**, 142–149 (2014).
6. Staub, I. & Sieber, S. A. Beta-lactam probes as selective chemical-proteomic tools for the identification and functional characterization of resistance associated enzymes in MRSA. *J. Am. Chem. Soc.* **131**, 6271–6276 (2009).
7. Frankel, M. B., Hendrickx, A. P., Missiakas, D. M. & Schneewind, O. LytN, a murein hydrolase in the cross-wall compartment of *Staphylococcus aureus*, is involved in proper bacterial growth and envelope assembly. *J. Biol. Chem.* **286**, 32593–32605 (2011).
8. Bukowski, M., Wladyka, B. & Dubin, G. Exfoliative toxins of *Staphylococcus aureus*. *Toxins (Basel)* **2**, 1148–1165 (2010).
9. Pietrocola, G., Nobile, G., Rindi, S. & Speziale, P. *Staphylococcus aureus* manipulates innate immunity through own and host-expressed proteases. *Front. Cell. Infect. Microbiol.* **7**, 166 (2017).
10. Böttcher, T. & Sieber, S. A. Beta-lactones as specific inhibitors of ClpP attenuate the production of extracellular virulence factors of *Staphylococcus aureus*. *J. Am. Chem. Soc.* **130**, 14400–14401 (2008).
11. Liu, Y., Patricelli, M. P. & Cravatt, B. F. Activity-based protein profiling: the serine hydrolases. *Proc. Natl Acad. Sci. USA* **96**, 14694–14699 (1999).
12. Patricelli, M. P., Giang, D. K., Stamp, L. M. & Burbaum, J. J. Direct visualization of serine hydrolase activities in complex proteomes using fluorescent active site-directed probes. *Proteomics* **1**, 1067–1071 (2001).
13. Simon, G. M. & Cravatt, B. F. Activity-based proteomics of enzyme superfamilies: serine hydrolases as a case study. *J. Biol. Chem.* **285**, 11051–11055 (2010).
14. Henness, S. & Perry, C. M. Orlistat: a review of its use in the management of obesity. *Drugs* **66**, 1625–1656 (2006).
15. Thornberry, N. A. & Weber, A. E. Discovery of JANUVIA (Sitagliptin), a selective dipeptidyl peptidase IV inhibitor for the treatment of type 2 diabetes. *Curr. Top. Med. Chem.* **7**, 557–568 (2007).
16. Kluge, A. F. & Petter, R. C. Acylating drugs: redesigning natural covalent inhibitors. *Curr. Opin. Chem. Biol.* **14**, 421–427 (2010).
17. Adam, G. C., Sorensen, E. J. & Cravatt, B. F. Chemical strategies for functional proteomics. *Mol. Cell. Proteomics* **1**, 781–790 (2002).
18. Leung, D., Hardouin, C., Boger, D. L. & Cravatt, B. F. Discovering potent and selective reversible inhibitors of enzymes in complex proteomes. *Nat. Biotechnol.* **21**, 687–691 (2003).
19. Jessani, N., Liu, Y., Humphrey, M. & Cravatt, B. F. Enzyme activity profiles of the secreted and membrane proteome that depict cancer cell invasiveness. *Proc. Natl Acad. Sci. USA* **99**, 10335–10340 (2002).
20. Ortega, C. et al. Systematic survey of serine hydrolase activity in *Mycobacterium tuberculosis* defines changes associated with persistence. *Cell Chem. Biol.* **23**, 290–298 (2016).
21. Tallman, K. R., Levine, S. R. & Beatty, K. E. Small-molecule probes reveal esterases with persistent activity in dormant and reactivating *Mycobacterium tuberculosis*. *ACS Infect. Dis.* **2**, 936–944 (2016).
22. Hatzios, S. K. et al. Chemoproteomic profiling of host and pathogen enzymes active in cholera. *Nat. Chem. Biol.* **12**, 268–274 (2016).
23. Zweerink, S. et al. Activity-based protein profiling as a robust method for enzyme identification and screening in extremophilic Archaea. *Nat. Commun.* **8**, 15352 (2017).
24. Hall, C. I. et al. Chemical genetic screen identifies *Toxoplasma* DJ-1 as a regulator of parasite secretion, attachment, and invasion. *Proc. Natl Acad. Sci. USA* **108**, 10568–10573 (2011).
25. Lentz, C. S. et al. Design of selective substrates and activity-based probes for Hydrolase Important for Pathogenesis 1 (HIP1) from *Mycobacterium tuberculosis*. *ACS Infect. Dis.* **2**, 807–815 (2016).
26. Cadieux, B., Vijayakumaran, V., Bernards, M. A., McGavin, M. J. & Heinrichs, D. E. Role of lipase from community-associated methicillin-resistant *Staphylococcus aureus* strain USA300 in hydrolyzing triglycerides into growth-inhibitory free fatty acids. *J. Bacteriol.* **196**, 4044–4056 (2014).
27. Rosenstein, R. & Gotz, F. Staphylococcal lipases: biochemical and molecular characterization. *Biochimie* **82**, 1005–1014 (2000).
28. Nguyen, M. T. et al. Staphylococcal (phospho)lipases promote biofilm formation and host cell invasion. *Int. J. Med. Microbiol.* https://doi.org/10.1016/j.ijmm.2017.11.013 (2017).
29. Staub, I. & Sieber, S. A. Beta-lactams as selective chemical probes for the in vivo labeling of bacterial enzymes involved in cell wall biosynthesis, antibiotic resistance, and virulence. *J. Am. Chem. Soc.* **130**, 13400–13409 (2008).
30. Fey, P. D. et al. A genetic resource for rapid and comprehensive phenotype screening of nonessential *Staphylococcus aureus* genes. *MBio* **4**, e00537–e12 (2013).
31. Utaida, S. et al. Genome-wide transcriptional profiling of the response of *Staphylococcus aureus* to cell-wall-active antibiotics reveals a cell-wall-stress stimulon. *Microbiology* **149**, 2719–2732 (2003).
32. Pietiäinen, M. et al. Transcriptome analysis of the responses of *Staphylococcus aureus* to antimicrobial peptides and characterization of the roles of vraDE and vraSR in antimicrobial resistance. *BMC Genomics* **10**, 429 (2009).
33. Sass, P. et al. The lantibiotic mersacidin is a strong inducer of the cell wall stress response of *Staphylococcus aureus*. *BMC Microbiol.* **8**, 186 (2008).
34. Muthaiyan, A. et al. Antimicrobial effect and mode of action of terpeneless cold-pressed Valencia orange essential oil on methicillin-resistant *Staphylococcus aureus*. *J. Appl. Microbiol.* **112**, 1020–1033 (2012).

35. Palazzolo-Ballance, A. M. et al. Neutrophil microbicides induce a pathogen survival response in community-associated methicillin-resistant *Staphylococcus aureus*. *J. Immunol.* **180**, 500–509 (2008).
36. Bore, E., Langsrud, S., Langsrud, O., Rode, T. M. & Holck, A. Acid-shock responses in *Staphylococcus aureus* investigated by global gene expression analysis. *Microbiology* **153**, 2289–2303 (2007).
37. Neumann, Y. et al. The effect of skin fatty acids on *Staphylococcus aureus*. *Arch. Microbiol.* **197**, 245–267 (2015).
38. Garland, M. et al. Development of an activity-based probe for acyl-protein thioesterases. *PLoS One* **13**, e0190255 (2018).
39. Jinno, A. & Park, P. W. Role of glycosaminoglycans in infectious disease. *Methods Mol. Biol.* **1229**, 567–585 (2015).
40. van Gemst, J. J. et al. RNA contaminates glycosaminoglycans extracted from cells and tissues. *PLoS One* **11**, e0167336 (2016).
41. Raz, A. & Fischetti, V. A. Sortase A localizes to distinct foci on the *Streptococcus pyogenes* membrane. *Proc. Natl Acad. Sci. USA* **105**, 18549–18554 (2008).
42. Mazmanian, S. K., Liu, G., Jensen, E. R., Lenoy, E. & Schneewind, O. *Staphylococcus aureus* sortase mutants defective in the display of surface proteins and in the pathogenesis of animal infections. *Proc. Natl Acad. Sci. USA* **97**, 5510–5515 (2000).
43. Clarke, A. J. & Dupont, C. O-Acetylated peptidoglycan: its occurrence, pathobiological significance, and biosynthesis. *Can. J. Microbiol.* **38**, 85–91 (1992).
44. Bera, A., Biswas, R., Herbert, S. & Gotz, F. The presence of peptidoglycan O-acetyltransferase in various staphylococcal species correlates with lysozyme resistance and pathogenicity. *Infect. Immun.* **74**, 4598–4604 (2006).
45. Brown, S. et al. Methicillin resistance in *Staphylococcus aureus* requires glycosylated wall teichoic acids. *Proc. Natl Acad. Sci. USA* **109**, 18909–18914 (2012).
46. Winstel, V. et al. Wall teichoic acid glycosylation governs *Staphylococcus aureus* nasal colonization. *MBio* **6**, e00632–15 (2015).
47. Weadge, J. T. & Clarke, A. J. Identification and characterization of O-acetylpeptidoglycan esterase: a novel enzyme discovered in *Neisseria gonorrhoeae*. *Biochemistry* **45**, 839–851 (2006).
48. Weadge, J. T., Pfeffer, J. M. & Clarke, A. J. Identification of a new family of enzymes with potential O-acetylpeptidoglycan esterase activity in both Gram-positive and Gram-negative bacteria. *BMC Microbiol.* **5**, 49 (2005).
49. Rahman, M. M. et al. The *Staphylococcus aureus* methicillin resistance factor FmtA is a d-amino esterase that acts on teichoic acids. *MBio* **7**, e02070–e15 (2016).
50. Garcia-Fernandez, E. et al. Membrane microdomain disassembly inhibits MRSA antibiotic resistance. *Cell* **171**, 1354–1367.e20 (2017).

Acknowledgements

We thank A. Horswill (University of Iowa) for sharing the GFP plasmid pCM29. We thank N. Amara and J. Yim for help with NMR analyses and S. Chen for LC-MS analysis of JCP678, and L. Popov, O. Zurek, J. Romaniuk and L. Cegelski for discussions. We also thank E. Yeh for access to the BD Accuri flow cytometer. C.S.L. was supported through a postdoctoral research fellowship by the German Research Foundation (DFG). This work was further supported through NIH grants 1R01GM111703 and R01EB026332 to M.B., 1R01GM117004 and 1R01GM118431-01A1 to E.W., 1R01AI101171 and 1R01AI069233 to E.P.S., and R21AI117255 to M.R.A.

Author contributions

C.S.L. and M.B. conceived the project. C.S.L designed and performed the in vitro experiments, synthesized compounds and analyzed data. J.R.S. designed and performed the in vivo infection experiments and the genetic manipulation of *S. aureus*, and analyzed data. L.A.C. and E.W. performed LC-MS/MS analysis. R.C. contributed to the comparative bacterial labeling experiments. M.G. synthesized compounds. M.R.A. contributed to the experimental design and analyzed data. E.P.S. designed and analyzed in vivo infection experiments. M.B. supervised the project, designed experiments and analyzed data. C.S.L. and M.B. wrote the manuscript, and all authors reviewed, discussed and edited the manuscript.

Competing interests

The authors declare no competing interests.

Additional information

Supplementary information is available for this paper at https://doi.org/10.1038/s41589-018-0060-1.

Reprints and permissions information is available at www.nature.com/reprints.

Correspondence and requests for materials should be addressed to M.B.

Publisher's note: Springer Nature remains neutral with regard to jurisdictional claims in published maps and institutional affiliations.

Methods

Bacterial strains and growth conditions. All bacterial strains employed in this study are summarized in Supplementary Table 4. *S. aureus* strains ATCC3555, USA300, Newman or its isogenic mutants were used as indicated. *S. aureus* and *S. epidermidis* were routinely cultured in Difco tryptic soy broth (TSB; BD, Sparks, MD), or on tryptic soy agar (TSA; BD). For compound screening and hit validation, strain ATCC3556 was grown on TSAMg (TSA with 100 mM $MgCl_2$) for 48–72 h. When required to select for transductants, erythromycin and lincomycin were added to the media at concentrations of 3 μg/mL and 20 μg/mL, respectively (Sigma Aldrich, St. Louis, MO). All incubations were performed at 37 °C, and liquid cultures were aerated by shaking at 180 r.p.m. unless indicated otherwise. The GFP plasmid pCM29[51] was obtained from Alexander Horswill (University of Iowa) and transformed into WT *S. aureus* Newman.

For growth curves of *S. aureus* Newman and its *fphB* transposon mutant, overnight cultures were diluted 1:400 in 30 mL fresh TSB and grown in 125-mL culture flasks at 180 r.p.m., 37 °C. Culture media included 1 μM JCP251 or the same volume (0.1%) of vehicle (DMSO) under control conditions. Culture aliquots were taken at 30–60 min intervals, diluted with TSB (1:1–1:3 dependent on the growth phase) and OD_{600} values were determined in a Laxco DSM-Micro Cell Densitometer.

S. typhimurium and *E. coli* were grown in Luria–Bertani (LB) broth or on LB agar. *L. monocytogenes* was grown in BHI broth or on BHI agar. *H. pylori* was grown in Brucella broth or on Columbia agar.

Cell lines and purification of peripheral mononuclear cells. RAW cells and HEK 293 cells were grown in Dulbecco's Modified Eagle Medium (supplemented with 10% Fetalplex Animal Serum Complex (Gemini Bio-Products), 2 mM L-glutamine and 1% penicillin/streptomycin). HepG2 cells were grown in DMEM with low glucose, L-glutamine and sodium pyruvate (Caisson Labs DML28), supplemented with 10% Fetalplex Animal Serum Complex and 1% penicillin/streptomycin. Cells were grown to 90% confluency, washed once with phosphate buffered saline (PBS) and harvested with a cell lifter. Cell pellets were centrifuged at 285*g* for 3 min and taken up in the desired culture medium. Whole human blood samples were received from the Stanford Blood Bank and peripheral mononuclear cells (PMNs) purified using the EasySep Direct Human Neutrophil Isolation Kit (StemCell Technologies).

Genetic manipulation of *S. aureus* strain Newman. Oligonucleotides used in confirming successful transduction of serine hydrolase mutants into *S. aureus* Newman can be found in Supplementary Table 5. In brief, transposon mutagenesis was used to generate insertion mutations in each of NWMN_0169, NWMN_0262, NWMN_0748, NWMN_1210, NWMN_1683, NWMN_2092, NWMN_2350, NWMN_2379, NWMN_2434, NWMN_2480, NWMN_2528 and NWMN_2569. Homologs of the aforementioned genes were first identified through the Basic Local Alignment Search Tool (BLASTn) in *S. aureus* USA300 FPR3757 (GenBank ID CP000255.1), and corresponding transposon mutants were identified and confirmed in the Nebraska Transposon Mutant Library[30] through PCR. The mutations were mobilized into *S. aureus* Newman using transduction with phage ϕ85. Successful transductants were confirmed through PCR and assessed for hemolysis relative to WT *S. aureus* Newman and USA300 by streaking on BD Trypticase Soy Agar II with 5% Sheep's Blood (BD).

FphB sequence analyses. The FASTA sequence of Q2FV90 (SAOUHSC_02844) was retrieved from UniProt and analyzed bioinformatically using the following web tools with settings for Gram-positive bacteria, if applicable: Secretome P2.0 (http://www.cbs.dtu.dk/services/SecretomeP/), PSORTB version 3.0.2 (http://www.psort.org/psortb/), Signal P4.1 (www.cbs.dtu.dk/services/SignalP/), Signal-3L 2.0 and MemBrain (http://www.csbio.sjtu.edu.cn/) and TmPred (minimum length: 14, maximum: 33) (http://www.ch.embnet.org/software/TMPRED_form.html).

Phylogenetic analysis. The FphB protein sequence (Uniprot ID: Q2FV90, strain NCTC8325, gene SAOUHSC_02844) was used as a BLASTp (protein–protein blast, https://blast.ncbi.nlm.nih.gov/) query sequence in a homology search against the nonredundant protein sequences database for different organisms. Top hits obtained for each organisms were subjected to a Clustal Omega Multiple Sequence Alignment (http://www.ebi.ac.uk/Tools/msa/clustalo/) and the phylogenetic tree was visualized using iTOL: interactive Tree Of Life (http://itol.embl.de/).

Cloning of SAOUHSC02844 (*fphB*) gene. Genomic DNA was purified from *S. aureus* ATCC35556 using the Qiagen DNEasy Blood & Tissue kit (Qiagen, Hilden, Germany) and used as a template for PCR amplification of the SAOUHSC_02844 gene using primers SAOUHSC02844_Fw_BamHI and SAOUHSC02844_Rv_XhoI with BamHI and XhoI restriction sites (Supplementary Table 5). The construct was cloned into the pET28a vector.

Expression, purification and labeling of rFphB. The pet28a-FphB expression vector was transformed into chemically competent BL21 (DE3) *E. coli*. An overnight culture of the transformed bacteria in LB + kanamycin 35 μg/mL selection medium was diluted 1:400 into 2 L selection medium (in a 4-L flask) at 37 °C, 220 r.p.m. At OD_{600} 0.1–0.2 growth was continued at 27 °C, and protein expression was induced at an OD_{600} of ~0.4 by addition of IPTG (10 μM final concentration). After growth for 3 h at 27 °C, 220 r.p.m., cells were harvested by centrifugation, transferred to two 50-mL conical tubes and centrifuged again, and bacterial pellets were stored at −80 °C.

Each pellet was thawed on ice, resuspended in 20 mL lysis buffer (50 mM NaH_2PO_4, 300 mM NaCl, 10 mM imidazole, 1% TritonX-10, pH 8.0) and lysed by sonication (six times for 10 s, 1.5 s pulse, 30% amplitude, Branson Sonifier). Lysates were centrifuged at 4,500 *g*, 4 °C for 45 min and the supernatant transferred to a 15-mL conical tube, and a 50% slurry of His60 Ni Superflow Resin (Clontech Laboratories) was added and incubated at room temperature (RT), rotating for 60 min, then purified by gravity flow. The resin was washed three times with 20 mM NaH_2PO_4, 300 mM NaCl, 20 mM imidazole, 1% TritonX-10, pH 8.0, and the His_6- and T7-tagged protein was eluted in 50 mM NaH_2PO_4, 300 mM NaCl, 200 mM imidazole. Eluates were labeled with 1 μM FP-TMR and analyzed by SDS–PAGE (TMR fluorescence scan and Coomassie stain). rFphB-containing fractions were pooled and further purified using the Novagen T7 Tag Affinity Purification Kit as per the manufacturer's instruction (EMD Millipore, Billerica, MA). Finally, purified rFphB was dialyzed twice into 50 mM Tris-HCl, 300 mM NaCl and glycerol was added to a final concentration of 10% for long-term storage at −80 °C. The concentration of purified rFphB was determined by A_{280} measurements using a calculated E1% of 10.76.

For ABP labeling experiments, rFphB (50 nM) in PBS/0.01% SDS was preincubated with different concentrations of JCP251 or DMSO for 30 min at 37 °C, before JCP251-bT (100 nM) or FP-TMR (1 μM) was added and the sample mixed by pipetting. Samples were incubated at for 37 °C for 30 min, boiled in SDS loading buffer and analyzed by SDS–PAGE.

Bacterial labeling with fluorescent ABPs. After growth on agar plate or in liquid culture as indicated, bacteria were suspended to the desired density in TSB and added to microtubes in a final volume of 50–300 μL. For inhibitor pretreatment experiments, the inhibitors were added from 100×-concentrated stock solutions in DMSO and incubated for 60 min (37 °C, 300 r.p.m.) before ABP-labeling. FP-TMR (1 μM) or JCP251-bT (10 nM or 100 nM) were added from 50–100× stock solutions in DMSO and cells incubated for 30 min, at 37 °C, 300 r.p.m. Samples were then taken up in SDS loading buffer and lysed by bead beating as described below.

For comparative bacterial labeling experiments, *H. pylori* and *L. monocytogenes* were grown in 5 mL of liquid culture. Cultures were spun down and cell densities adjusted to ~2×10^8 CFU per 100 μL in TSB. All other bacterial strains were scraped off agar plates and resuspended in TSB at equivalent concentrations. To 100-μL aliquots of bacterial suspension was added 1 μL of 100 μM FP-TMR or 10 μM JCP251-bT. Cells were mixed by pipetting and incubated at 37 °C for 30 min. PBS (1 mL) was added and samples were centrifuged (8,000 *g*, 5 min, RT). The supernatant was taken off and cell pellets resuspended in 500 μL SDS loading buffer and lysed by bead beating.

Competitive activity-based protein profiling screen. Experimental details on the screening procedure are given in the Small Molecule Screening Data Table (Supplementary Table 1).

Bacterial lysis. After probe labeling, bacterial suspensions were prepared in PBS/0.1% SDS or immediately in SDS loading buffer. Suspensions were transferred to 0.6 mL (400–500 μL samples) or 2.0 mL (1.0–1.2 mL samples) O-ring tubes approximately half-filled with 0.1 mm glass beads (Biospec Products, Bartlesville, OK, USA). Tubes were placed in a prechilled aluminum vial rack and samples lysed in a Mini-BeadBeater-96 (Biospec Prod) (three times for 50 s with 2 min resting on ice in between) and centrifuged at 13,000 *g*, 4 °C, 5 min.

SDS–PAGE analysis of samples labeled with fluorescent ABPs. Lysate supernatants were combined with 4× SDS loading buffer. Samples were boiled at 95 °C for 10 min and separated by SDS–PAGE gel. TMR fluorescence was scanned on a Typhoon 9410 variable mode imager (TAMRA channel, $\lambda_{ex} = 380$, 580 BP filter).

Preparation of RAW cell lysates and fractionation. At ~90% confluency, RAW cells were washed twice in PBS, scraped off plates and harvested in DMEM plus 2 mM L-glutamine. Cells were centrifuged at 285*g*, RT, and adjusted to a concentration of 10^5 cells per 50 μL. Cell suspensions were cooled on ice, transferred into 7-mL vials filled with ~3.5 mL of 0.1 mm glass beads and lysed by bead beating for 50 s. Supernatants were stored at −80 °C or further fractionated by ultracentrifugation at 100,000 *g*, 60 min, 4 °C in a Optima MAX-TL Ultracentrifuge (Beckman Coulter, Indianapolis, IN, USA).

ABP labeling experiments in eukaryotic and bacterial cell cocultures. *Labeling to assess the selectivity of JCP251-bT.* RAW cells or PMNs (~50,000) were seeded in RPMI/HEPES into sterile flat-bottom 96-well plates. The plate was spun down at 285*g* (accel = 5, brake = 3) for 3 min and incubated at 37 °C, 5% CO_2 for 60 min. *S. aureus* ATCC3556 was grown overnight on TSA, scraped off the plate and adjusted to an OD_{600} of 0.5 in DMEM (+2 mM L-glutamine). Bacterial suspension

(80 µL, 1×10^7 CFU, MOI = 200) or medium were added to either cell type or control wells containing medium only and incubated for 60–90 min at 37 °C, 5% CO_2, before JCP251-bT was added to a final concentration of 100 nM. Plates were spun down, incubated at 37 °C, 5% CO_2. 60 µL 4× SDS loading buffer was added to lyse eukaryotic cells. Samples were transferred to O-ring-tubes for lysis and SDS–PAGE analysis.

FphB stimulation experiments. *S. aureus* ATCC35556 was harvested after growth on TSA or *S. aureus* Newman was grown to exponential phase in TSB and centrifuged. Bacteria were resuspended in serum- and antibiotic free culture medium (DMEM, 2 mM L-glutamine or RPMI, 5 mM HEPES) and incubated for 60–90 min in the presence of different stimulatory conditions before labeling with 50–100 nM JCP251-bT. Stimulatory conditions included RAW cells or PMNs seeded in serum- and antibiotic free culture medium; fixed RAW, HEK 293 or HepG2 cells (treated with 2% PFA for 10 min and washed three times with PBS); Fetalplex Serum (before and after extraction with an equal volume of chloroform); and full RAW cell lysate or soluble and insoluble fractions after ultracentrifugation, as well as heat-inactivated lysate fractions. Heat-inactivation of lysate fractions was done at 95 °C for 15 min. After probe labeling, cell lysis and SDS–PAGE analysis FphB bands were quantified using Image Studio Lite software (LI-COR Biosciences). Statistical analysis was done using Prism 7.0 (GraphPad Software)

Fluorogenic substrate assays. Stock solutions of 4-methylumbelliferyl (4-MU)-based fluorogenic substrates were dissolved in DMSO (1 mM) and 0.3 µL were added to the wells of an opaque flat-bottom 384-well plate. Thirty microliters of a solution rFphB in PBS/0.01% TritonX-100 (400 pM active enzyme) was added and fluorescence ($\lambda_{ex}=365$ nm and $\lambda_{em}=455$ nm) was read at 37 °C in 1-min intervals on a Cytation 3 imaging reader (BioTek, Winooski, VT, USA) for 60 min. Turnover rates in the linear phase of the reaction (10–40 min) were calculated using Gen5 software (BioTek) as RFU/min. Rates were normalized by subtracting background hydrolysis rates measured for each substrate in reaction buffer in the absence of protein.

Determination of inactivation constants k_{obs}/[I]. Inactivation rates k_{obs}/[I] of recombinant FphB by inhibitors JCP251 and JCP251-bT were measured under pseudo-first-order conditions at a substrate concentration of 1 mM 4-MU butyrate. To 0.3 µL substrate in DMSO were added 0.3 µL of inhibitor (in DMSO) in the wells of a 384-well plate and, after addition of 29.6 µL FphB (0.8 nM active enzyme) in PBS/0.01% TritonX-100, the enzymatic reaction was monitored as described above at 37 °C for 30 min. Data were normalized by subtracting background signal due to substrate hydrolysis (in the absence of FphB) at each time point. The normalized progress curve was fit to the formula $P=V/k_{app}(1-e^{-k_{app}t})+C$, with P = product formation, V = initial velocity, t = time and k_{app} as the apparent rate constant. A constraint was set for V as the rate determined for the linear, uninhibited reaction for each experiment. The second order rate constant k_{obs}/[I] was then calculated using the formula $k_{obs}/[I]=(k_{app}/[I])(1+[S]/K_M)$ for three different inhibitor concentrations (5 nM, 10 nM and 20 nM). The K_M value for this substrate was experimentally determined as 52 ± 11 µM. Mean k_{obs}/[I] values ± s.d. were determined from 3 independent experiments.

FITC-casein assay. A stock solution of FITC-casein (5 mg/mL in water) was diluted 1:500 in assay buffer (PBS/0.01% Triton X-100) and 50 µL added to the wells of an opaque flat-bottom 96-well plate. Fifty microliters FphB (2 nM active enzyme), trypsin (2 nM) or assay buffer were added and the plate incubated at 37 °C. After 30 min and overnight incubation, fluorescein fluorescence ($\lambda_{ex}=485$ nm and $\lambda_{em}=538$ nm) was measured on a Cytation 3 imaging reader.

FP-biotin labeling of *S. aureus* serine hydrolases and sample preparation for mass spectrometry. *S. aureus* ATCC35556 was grown on TSBMg for 72 h and resuspended to an OD_{600} of ~100 in 13 mL TSB. Aliquots of 1 mL were transferred to a 1.5-mL tube and JCP251 (300 nM, 1 µM), JCP678 (1 µM) or DMSO (5 µL) was added and cells incubated for 60 min at 37 °C, 700 r.p.m. FP-biotin (5 µL, 1 mM in DMSO) was added to the bacteria and incubated for 30 min before samples were spun down (4,500 *g*, 5 min, 4 °C) and the supernatant was aspirated. The cell pellet was resuspended in 1.2 mL PBS/0.1% SDS, and 100 µL Protease Inhibitor Cocktail were added. The samples were transferred to 2-mL O-ring tubes half-filled with 0.1 mm glass beads and the tubes placed into prechilled aluminum blocks and lysed by bead-beating (three times for 50 s with 2 min on ice in between) as described above. Samples were centrifuged for 5 min at 10,000 *g*, 4 °C. Aliquots of 15 µL were taken for SDS–PAGE analysis and SA-HRP blot. Protein concentration in the supernatant was adjusted to 0.8 mg/mL and 200 µL 10% TritonX-100 added to 0.8 mg of proteome and incubated at 4 °C for 1 h, rotating. Sample volume was brought to 2.5 mL and added to a pre-equilibrated PD10 desalting column (GE LifeSciences), discarding the flowthrough. Samples were eluted with 3.5 mL PBS and 10% SDS/PBS was added to a final concentration of 0.5% SDS. Samples were boiled at 90 °C for 8 min, then cooled in a –20 °C freezer for ~5 min before ~80 µL of a prewashed 50% streptavidin-agarose slurry was added and samples were incubated at RT for 1 h, rotating. Samples were centrifuged at 300 *g* for 2 min and washed twice with 1% SDS, twice with 6 M urea and twice with PBS (each 10 mL). After the final wash, resin was resuspended in 500 µL 6 M urea, 25 µL of DTT (30 mg/mL solution in PBS) and heated at 65 °C for 15 min. Iodoacetamide (25 µL, 14 mg/mL in PBS) was added and incubated at 37 °C for 30 min. Following incubation, 950 µL PBS was added, the resin spun down and the supernatant discarded. A premixed solution of 200 µL of 2 M urea/PBS, 2 µL 100 mM $CaCl_2$ in water and 4 µL trypsin solution (20 µg lyophilized powder reconstituted in 40 µL 2 M urea/PBS) was added to the resin and samples incubated at 37 °C overnight, rotating. Tryptic peptide digests were separated from the resin over a spin-filter column and resin washed twice with 50 µL PBS. Formic acid (15 µL) was added to the combined eluates for each sample. Samples were stored at –20 °C until LC/LC-MS/MS analysis.

Liquid chromatography–mass spectrometry analysis. LC/LC-MS/MS analysis was performed on an LTQ-Orbitrap Discovery mass spectrometer (ThermoFisher) coupled to an Agilent 1200 series HPLC. Peptide digests were pressure loaded onto a 250-µm fused silica desalting column packed with 4 cm of Aqua C18 reverse phase resin (Phenomenex). The peptides were eluted onto a biphasic column (100 µm fused silica with a 5-µm tip, packed with 10 cm C18 and 4 cm Partisphere strong cation exchange resin (SCX, Whatman)) using a gradient of 5–100% buffer B in buffer A (buffer A: 95% water, 5% acetonitrile, 0.1% formic acid; buffer B: 20% water, 80% acetonitrile, 0.1% formic acid). The peptides were then eluted from the SCX onto the C18 resin and into the mass spectrometer using four salt steps previously described[52]. The flow rate through the column was set to ~0.25 µL/min and the spray voltage was set to 2.75 kV. One full MS scan (FTMS) (400–1,800 MW) was followed by eight data-dependent scans (ITMS) of the *n*th most intense ions.

The tandem MS data were searched using the SEQUEST algorithm using a concatenated target/decoy variant of the NCTC8325 *S. aureus* UniProt database. A static modification of + 57.02146 on cysteine was specified to account for alkylation by iodoacetamide. SEQUEST output files were filtered using DTASelect. Proteins with less than five average spectral counts among the three replicates of the control sample were filtered from the dataset. Fold change was calculated as the quotient of the number of average spectral counts for the control sample divided by the number of average spectral counts for the compound treated sample. *P* values were calculated for the compound treated samples and control samples.

Flow cytometry. Labeled bacteria were washed twice in PBS, fixed in 2% PFA for 10 min and washed three times with PBS. Bacteria were resuspended in PBS and analyzed on a BD Accuri RUO Special Order System Flow Cytometer with BD CSampler software (BD Biosciences, San Diego, USA). FSC-A threshold was set to 5,000 and 30,000–50,000 events in the bacterial cell gate were recorded. Bodipy-TMR fluorescence was detected using a 552 nm laser and 586 nm filter (FL2-detector).

Fluorescence microscopy. *Imaging of RAW cells*. RAW cells (1×10^5) were seeded onto a sterile coverslip in a 24-well plate in 400 µL DMEM + 2.5 mM L-glutamine and incubated at 37 °C, 5% CO_2. The next day *S. aureus* ATCC3556 cells were harvested after growth on TSAMg and adjusted to an OD_{600} of ~0.8 in DMEM (+2.5 mM L-glutamine). Fifty microliters (1×10^7 CFU) were added to the cells and incubated for 60 min at 37 °C, 5% CO_2, before 5 µL of 7 µM JCP251-bT (100 nM) was added and cells incubated for another 30 min at 37 °C, 5% CO_2. After 30 min of labeling, cells were washed twice with PBS, fixed in 2% PFA for 10 min at RT and washed three times with PBS. Coverslips were mounted onto microscope slides with Vectashield Antifade Mounting Medium with DAPI (Vector Laboratories).

Imaging of bacteria only. A suspension of labeled and fixed bacteria in PBS was added to an agarose pad on a microscope slide and covered with a coverslip. Cells were imaged at 63× using a Zeiss LSM 700 confocal microscope in the bodipy-TMR and GFP channels. Laser and gain settings were configured at the beginning of each experiment and constant settings used for all samples.

Murine model of *S. aureus* systemic infection. Two days before infection, *S. aureus* Newman and its isogenic transposon mutants were streaked on TSA and incubated overnight at 37 °C. Single isolated colonies from the TSA plates were used to prepare overnight cultures in 5 mL of TSB. Overnight cultures were back-diluted 1:100 in 5 mL of TSB and grown for 2.5 h to mid-exponential phase. Cultures were pelleted by centrifugation at 5,916*g* for 10 min and washed once in sterile PBS. Cells were normalized to an OD_{600} of 0.4 in PBS, corresponding to a cell density of approximately $1–2\times10^8$ CFU/mL. Each inoculum was quantified by serial dilution and plating on TSA.

For all mouse experiments, female BALB/cJ mice were purchased from The Jackson Laboratory and infected at 6–8 weeks of age. In brief, mice were anesthetized by intraperitoneal injection with 125–250 mg/kg of 2,2,2-tribromoethanol and were subsequently infected with *S. aureus* through injection of 100 µL of prepared cells (~$1–2\times10^7$ total CFU) into the retroorbital sinus. The infection was allowed to proceed for 96 h, with frequent monitoring throughout the course of the experiment. The mice were assessed for health and weight every 12 and 24 h, respectively. Following euthanasia by CO_2 inhalation, the kidneys, heart and liver were extracted. The organs were homogenized and serially diluted in sterile PBS before plating for CFU on TSA. Plates were incubated

overnight at 37 °C and counted the following day. All mouse experiments were evaluated and approved by the Institutional Animal Care and Use Committee (IUCAC) of Vanderbilt University Medical Center and are in compliance with NIH guidelines, the Animal Welfare Act and US Federal law.

In vivo inhibitor studies. To assess for function of the JCP251 inhibitor in vivo, *S. aureus* WT and *fphB*::ϕNΣ cells were prepared as described above. Following washing and normalization in PBS, the inocula were mixed with 1 μM of the JCP251 inhibitor and incubated with shaking at room temperature for 1 h. Mice were injected with 100 μL of the *S. aureus*–inhibitor mix, or with 100 μL of *S. aureus* in PBS with 1% DMSO as a mock control for the inhibitor. The infection was allowed to proceed as above and bacterial burdens in the kidneys, liver and hearts were assessed after 96 h.

Statistical analyses. All statistical analyses were done using GraphPad Prism 7 (GraphPad Software Inc.). Details on sample size and statistical tests used are given in the corresponding figure legends. Unless stated otherwise, data from in vitro experiments subject to statistical analysis was performed in three technical replicates and analyzed by unpaired Student's *t*-test. Representative data shown were obtained at least in two independent experiments with a similar outcome. Data from *S. aureus* infection experiments were pooled from two or three different experiments. If nonparametric one-way ANOVA (Kruskal–Wallis test) indicated that median values of the different experimental groups within a dataset varied significantly, individual groups were compared by pairwise significance testing using unpaired, two-tailed Mann–Whitney *U* test. *P*-values < 0.05 were considered significant.

Reporting Summary. Further information on experimental design is available in the Nature Research Reporting Summary.

Data availability and code availability. The mass spectrometry proteomics data have been deposited to the ProteomeXchange Consortium via the PRIDE partner repository with the dataset identifier PXD009210 (https://www.ebi.ac.uk/pride/archive/).

References

51. Pang, Y. Y. et al. agr-dependent interactions of *Staphylococcus aureus* USA300 with human polymorphonuclear neutrophils. *J. Innate Immun.* **2**, 546–559 (2010).
52. Weerapana, E., Speers, A. E. & Cravatt, B. J. Tandem orthogonal proteolysis-activity-based protein profiling (TOP-ABPP)-a general method for mapping sites of probe modification in proteomes. *Nat. Protoc.* **2**, 1414–1425 (2007).